Remodelling of biological tissues with fibre recruitment and reorientation in the light of the theory of material uniformity

Remodelling of Biological Tissues with Fibre Recruitment and Reorientation in the Light of the Theory of Material Uniformity

Amir Hamedzadeh[a], Alfio Grillo[b], Marcelo Epstein[a], Salvatore Federico[a,*]

[a] *Department of Mechanical and Manufacturing Engineering, The University of Calgary*
2500 University Drive NW, Calgary, Alberta, T2N1N4, Canada
[b] *Department of Mathematical Sciences "G.L. Lagrange", Dipartimento di Eccellenza 2018-2022, Politecnico di Torino*
Corso Duca degli Abruzzi 24, 10124, Torino, Italy

Abstract

This study focusses on the remodelling of biological tissues in the framework of the theory of material uniformity. A constitutive evolution model is introduced, including fibre recruitment and reorientation, and subjected to the entropy inequality, which enforces the Second Principle of Thermodynamics. The model is applied to a numerical example describing a pressurised fibre-reinforced cylinder, roughly representing an artery, and is able to capture the major characteristics of remodelling in arteries, as reported in the literature.

Keywords: collagen fibre; recruitment; remodelling; growth; material uniformity

1. Introduction

Growth and remodelling in biological tissues can be studied as *anelastic phenomena*. Anelastic processes, such as plasticity or growth-remodelling, are accompanied by a change in microstructure resulting in *configurational forces* and residual stresses (e.g., Hoger, 1997; Gurtin, 1999). While plasticity occurs at constant mass, biological tissues not only experience a change in microstructure, but also an increase (growth) or decrease (resorption) of mass. Among the first attempts to approach the problem of growth and remodelling from the continuum mechanical perspective are the seminal works by Cowin and Hegedus (1976) and Hegedus and Cowin (1976) on bone remodelling. Rodriguez et al. (1994) studied growth and remodelling in arteries and used the Bilby-Kröner-Lee decomposition of the deformation gradient $\boldsymbol{F}$ into a growth part $\boldsymbol{F}_g$ and an elastic part $\boldsymbol{F}_e$. In practice, they considered a residually stressed reference configuration which grows into a stress-free intermediate (and generally incompatible) configuration, and finally deforms elastically to the current (and compatible) configuration actually attained by the body. Moreover, the fact that the collagen fibres in a biological tissue may be undulated in the reference configuration, and will thus bear stress only after a certain threshold stretch, has been studied as an additional remodelling parameter for the case of aneurysms (Watton et al., 2004; Watton and Hill, 2009).

Here we employ the framework proposed by Epstein and Maugin (2000), in which growth and remodelling are seen as the two aspects of an evolution process implying a local rearrangement of material inhomogeneities, described in terms of an *implant*, under the light of the *theory of material uniformity*. In this framework, growth and remodelling are governed by the *inhomogeneity rate*, $\boldsymbol{L_P} = \dot{\boldsymbol{P}}\boldsymbol{P}^{-1}$, where $\boldsymbol{P}^{-1}$ formally corresponds to the growth tensor $\boldsymbol{F}_g$ of Rodriguez et al. (1994). Specifically, the trace of $\boldsymbol{L_P}$ is often required to be proportional to the source or sink of mass due to growth that features in the local mass balance of the body. Given $\boldsymbol{L_P}$, the implant tensor $\boldsymbol{P}$ can be determined by integrating the differential equation $\dot{\boldsymbol{P}} = \boldsymbol{L_P}\boldsymbol{P}$. However, the way in which $\boldsymbol{L_P}$ is supplied is not unique.

We had previously modelled the effect of the undulation of the individual fibrils in a collagen fibre (Hamedzadeh et al., 2018) and, in this study, we employ the same mechanism for an entire fibre, and in terms of the theory of material uniformity. Therefore, we introduce the proper material implant describing both reorientation and recruitment of the fibres in an artery, and solve the benchmark problem previously studied by Grillo et al. (2015) in order to elucidate our results.

2. Theory of Uniformity

We follow the *theory of uniformity*, originally introduced by Noll (1967) and further developed by Epstein and Maugin (1990). A material body $\mathcal{B}$ is said to be *uniform* if all of its points are made of the *same* material. This implies that the tangent spaces $T_X\mathcal{B}$ of the points X of $\mathcal{B}$ have been modelled on an archetypal vector space $\mathcal{A} \equiv \mathbb{R}^3$, called precisely the *archetype*, via an isomorphism

$$\boldsymbol{P}(X) : \mathcal{A} \to T_X\mathcal{B}, \tag{1}$$

*Corresponding author
Email address: salvatore.federico@ucalgary.ca (Salvatore Federico)

at every point X. In other words, if we look at the microscopic structures surrounding two materially uniform points X and Y, we might not see identical pictures, as one might have been distorted or rotated in a different manner than the other. However, we can pass from X to Y via $\boldsymbol{P}(Y)\,\boldsymbol{P}^{-1}(X) : T_X\mathcal{B} \to T_Y\mathcal{B}$. For this reason, $\boldsymbol{P}$ is called the *material isomorphism*.

Now, suppose to have an elastic material with elastic potential $W(X,t) = \hat{W}(\boldsymbol{F}(X,t), X, t)$ depending explicitly on the point X and time t. If the body is uniform, then the elastic potential depends on the point X and time t only through the (in this case, time-dependent) uniformity field $\boldsymbol{P}$, i.e.,

$$\hat{W}(\boldsymbol{F}(X,t), X, t) = J_{\boldsymbol{P}}^{-1}(X,t)\,\check{W}(\boldsymbol{F}(X,t)\boldsymbol{P}(X,t)), \quad (2)$$

where $\check{W}$ is the elastic potential in the archetype, and $J_{\boldsymbol{P}}^{-1}$ comes from the theorem of the change of variables (Epstein and Maugin, 1990).

3. Material Implant for a Single Fibre

The generic fibre is straight with no undulation in the archetype, and the implant $\boldsymbol{P}(X,t)$ rotates the fibre, crimps it and maps it into the tangent space $T_X\mathcal{B}$ at X, as shown in Figure 1. Note that using the implant $\boldsymbol{P}$ is equivalent to assuming the existence of a non-compatible intermediate configuration, which is mapped onto by the *straightening deformation* $\boldsymbol{F}_s$ coming from the multiplicative decomposition $\boldsymbol{F} = \boldsymbol{F}_e\boldsymbol{F}_s$ (Hamedzadeh et al., 2018).

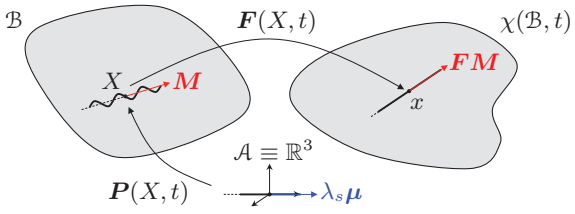

Figure 1: Collagen fibre recruitment seen in terms of the theory of uniformity, with the straightened fibre in the archetype.

The archetypal straightened fibre is represented by the vector $\lambda_s\boldsymbol{\mu}$, where $\boldsymbol{\mu}$ is a unit vector and λ_s is the straightening stretch needed to map a fibre from its referential crimped state back to the archetypal straight state. The uniformity field $\boldsymbol{P}$ maps the archetypal vector $\lambda_s\boldsymbol{\mu}$ into the unit referential vector $\boldsymbol{M}$. Application of the polar decomposition theorem to $\boldsymbol{P}$ yields

$$\boldsymbol{P} = \boldsymbol{R}\boldsymbol{U} = \boldsymbol{R}\hat{\boldsymbol{U}}(\lambda_s), \quad P^A{}_\beta = R^A{}_\alpha\, U^\alpha{}_\beta, \quad (3)$$

where $\boldsymbol{R}$ rotates and shifts the fibre vector $\boldsymbol{\mu} \in \mathcal{A}$ from the archetype to the referential vector $\boldsymbol{M} \in T_X\mathcal{B}$, and $\boldsymbol{U} = \hat{\boldsymbol{U}}(\lambda_s)$ is the crimping experienced by the fibre when passing from the straight archetypal configuration to the undulated referential one. In order to find the expressions of $\boldsymbol{R}$ and $\boldsymbol{U}$, we need some geometrical preliminaries.

Let $\mathfrak{g}$ be a metric in the archetype $\mathcal{A}$ and $\{\mathfrak{a}_\alpha\}_{\alpha=1}^3$ a $\mathfrak{g}$-orthonormal basis of $\mathcal{A}$. Since the body $\mathcal{B}$ is a *trivial* manifold embedded in the affine space $\mathcal{S} \equiv \mathbb{E}^3$, we can afford the luxury of choosing Cartesian coordinates $\{Z^\alpha\}$, such that the associated basis $\{\boldsymbol{I}_\alpha\}_{\alpha=1}^3$ coincides with the archetypal basis $\{\mathfrak{a}_\alpha\}_{\alpha=1}^3$ at every tangent space $T_X\mathcal{B}$. We also choose a system of curvilinear coordinates $\{X^A\}$ in the body $\mathcal{B}$, with associated basis $\{\boldsymbol{E}_A\}_{A=1}^3$. The change of basis and the transformation rule for vectors are

$$\boldsymbol{E}_A = \frac{\partial Z^\alpha}{\partial X^A}\,\boldsymbol{I}_\alpha, \qquad W^A = \frac{\partial X^A}{\partial Z^\alpha}\,W^\alpha. \quad (4)$$

Consider the vector $\tilde{\boldsymbol{M}} \in \mathcal{A}$ such that its components are equal to the Cartesian components of $\boldsymbol{M} \in T_X\mathcal{B}$, i.e., $\tilde{M}^\alpha = M^\alpha$. The orthogonal tensor $\boldsymbol{R}$ is obtained as

$$R^A{}_\beta = \frac{\partial X^A}{\partial Z^\alpha} Q^\alpha{}_\beta, \quad (5)$$

where $Q^\alpha{}_\beta$ are the components of the archetypal tensor $\boldsymbol{Q}$ rotating the archetypal direction $\boldsymbol{\mu}$ into $\tilde{\boldsymbol{M}}$. The corresponding matrix $[\![\boldsymbol{Q}]\!]$ is found as a function of the unit vector $\boldsymbol{\omega} = \boldsymbol{\mu} \times \tilde{\boldsymbol{M}}/\|\boldsymbol{\mu} \times \tilde{\boldsymbol{M}}\|$, which describes the axis of rotation, and the amplitude $\theta = \arccos(\boldsymbol{\mu}.\tilde{\boldsymbol{M}})$ of the rotation. Then, the rotation matrix $[\![\boldsymbol{Q}]\!]$ can be obtained by exponentiating the skew-symmetric matrix $[\![\boldsymbol{\Omega}]\!]$ associated with the vector $\boldsymbol{\omega}$, i.e.,

$$[\![\boldsymbol{Q}]\!] = e^{[\![\boldsymbol{\Omega}]\!]\theta}, \qquad \Omega^\alpha{}_\gamma = \epsilon^\alpha{}_{\beta\gamma}\omega^\beta, \quad (6)$$

which can be conveniently expressed by Rodriguez' formula (Koks, 2006) as

$$Q^\alpha{}_\gamma = \delta^\alpha{}_\gamma + (\sin\theta)\,\Omega^\alpha{}_\gamma + (1-\cos\theta)\,\Omega^\alpha{}_\beta\,\Omega^\beta{}_\gamma. \quad (7)$$

The components of the pure stretch $\boldsymbol{U}$ are given by

$$U^\alpha{}_\beta = (\lambda_s^{-1} - 1)\mu^\alpha\mu_\beta + \delta^\alpha{}_\beta, \quad (8)$$

where $\mu_\beta = \mathfrak{g}_{\beta\gamma}\,\mu^\gamma$ are the components of the covector $\boldsymbol{\mu}^\flat$ associated with $\boldsymbol{\mu}$ via the archetypal metric $\mathfrak{g}$. Finally, the material implant $\boldsymbol{P}$ is given by

$$P^A{}_\gamma = \frac{\partial X^A}{\partial Z^\alpha} Q^\alpha{}_\beta \left[(\lambda_s^{-1} - 1)\mu^\beta\mu_\gamma + \delta^\beta{}_\gamma\right], \quad (9)$$

which can be simplified into

$$P^A{}_\gamma = (\lambda_s^{-1} - 1)\,M^A\mu_\gamma + \frac{\partial X^A}{\partial Z^\alpha} Q^\alpha{}_\gamma, \quad (10)$$

since $Q^\alpha{}_\beta\,\mu^\beta = \tilde{M}^\alpha$ and $(\partial X^A/\partial Z^\alpha)\,\tilde{M}^\alpha = M^A$. For an *isochoric* implant $\boldsymbol{P}$ (i.e., *pure* remodelling, *no* growth, see Epstein and Elzanowski, 2007), the stretch $\boldsymbol{U}$ must be changed into

$$U^\alpha{}_\beta = (\lambda_s^{-1} - \lambda_s^{1/2})\mu^\alpha\mu_\beta + \lambda_s^{1/2}\,\delta^\alpha{}_\beta, \quad (11)$$

so that we have

$$P^A{}_\gamma = (\lambda_s^{-1} - \lambda_s^{1/2})\,M^A\mu_\gamma + \lambda_s^{1/2}\,\frac{\partial X^A}{\partial Z^\alpha} Q^\alpha{}_\gamma. \quad (12)$$

4. Material Implant for a Distribution of Fibres

We assume that the fibres in our biological tissue have a statistical distribution of orientation. Thus, rather than implanting fibres individually, we can implant a whole family of statistically oriented fibres into a material point X. We also assume that the elastic potential $\hat{W}_f$ of the fibres is the sum of an isotropic part $\hat{W}_{fi}$ and an anisotropic part $\hat{W}_{fa}$. With an abuse of notation, we do not indicate the arguments (X,t) of the tensor fields, and write the anisotropic *ensemble* elastic potential of the fibres (Federico and Herzog, 2008) as

$$\hat{W}_e(\boldsymbol{C},X,t)=\int_{\mathbb{S}^2_X\mathcal{B}}\hat{W}_{fa}(\hat{I}_4,X,t)\;\Psi(\boldsymbol{M};X,t), \qquad (13)$$

where $\hat{I}_4=\boldsymbol{C}:(\boldsymbol{M}\otimes\boldsymbol{M})$ is the fourth invariant of the right Cauchy-Green deformation $\boldsymbol{C}$ along the vector $\boldsymbol{M}$, and the probability distribution Ψ depends explicitly on X and t. Following the definition (2) of material uniformity, the fibre elastic potential $\hat{W}_{fa}$ is related to its archetypical counterpart by

$$\hat{W}_{fa}(\hat{I}_4,X,t)=J_{\boldsymbol{P}}^{-1}\;\check{W}_{fa}(\check{I}_4), \qquad (14)$$

where $\check{I}_4=\boldsymbol{P}^T\boldsymbol{C}\boldsymbol{P}:\boldsymbol{\mu}\otimes\boldsymbol{\mu}$ is the fourth invariant of $\boldsymbol{P}^T\boldsymbol{C}\boldsymbol{P}$ along the vector of $\boldsymbol{\mu}$. Thus, Eq. (13) becomes

$$\hat{W}_e(\boldsymbol{C},X,t)=J_{\boldsymbol{P}}^{-1}\int_{\mathbb{S}^2}\check{W}_f(\check{I}_4)\,\check{\Psi}(\boldsymbol{\mu}), \qquad (15)$$

where $\mathbb{S}^2$ denotes the archetypical unit sphere and $\check{\Psi}$ is the archetypal probability distribution.

5. Dissipation Inequality and Evolution Law

An evolution equation is required as an additional differential equation providing the inhomogeneity rate $\boldsymbol{L}_{\boldsymbol{P}}=\dot{\boldsymbol{P}}\boldsymbol{P}^{-1}$ as a function of all quantities that can act as driving forces of the evolution process, i.e.,

$$\boldsymbol{L}_{\boldsymbol{P}}(X,t)=\hat{\mathcal{F}}(\boldsymbol{P}(X,t),\mathfrak{A}(X,t),X), \qquad (16)$$

where $\mathfrak{A}$ represents all possible driving force arguments, such as Eshelby stress, $\mathfrak{E}=W\boldsymbol{I}^T-\boldsymbol{F}^T\boldsymbol{T}$, or Mandel stress, $\mathfrak{M}=\boldsymbol{F}^T\boldsymbol{T}$, $\boldsymbol{T}$ being the first Piola-Kirchhoff stress. Note that, here, $\hat{\mathcal{F}}$ does not depend on time explicitly, i.e., it is *autonomous* with respect to time.

As shown by Epstein and Maugin (2000) and Epstein and Elzanowski (2007), and mentioned in the Introduction, there are some restrictions that are essential for an appropriate choice of evolution law. First, the evolution law should be invariant with respect to a change of reference configuration. Such an evolution law is said to be *reduced to the archetype* and reads

$$\boldsymbol{L}_{\boldsymbol{P}}=\dot{\boldsymbol{P}}\boldsymbol{P}^{-1}=\check{\mathcal{F}}(J_{\boldsymbol{P}}\,\boldsymbol{P}^T\,\mathfrak{A}\,\boldsymbol{P}^{-T}). \qquad (17)$$

Second, the evolution law should satisfy the dissipation inequality, i.e., within a purely mechanical framework and for a hyperelastic material, for which the first Piola-Kirchhoff stress tensor $\boldsymbol{T}$ is given by $\boldsymbol{T}=(\partial\hat{W}/\partial\boldsymbol{F})(\boldsymbol{F})$, the dissipation $\mathfrak{D}$ per unit reference volume satisfies (Epstein and Elzanowski, 2007)

$$\mathfrak{D}=-\dot{W}+\boldsymbol{T}:\dot{\boldsymbol{F}}=-\mathfrak{M}:\boldsymbol{L}_{\boldsymbol{P}}\geq 0. \qquad (18)$$

The same result has been found with the BKL decomposition in several works on inelastic processes (see e.g., Simo and Hughes, 1986; Simo, 1988; Cleja-Tigoiu and Maugin, 2000; Imatani and Maugin, 2002; Grillo et al., 2018; Di Stefano et al., 2018; Crevacore et al., 2018). Here, we assume a rate-dependent type of remodelling and reformulate $\mathfrak{D}=\hat{\mathfrak{D}}(\boldsymbol{C},\boldsymbol{P},\boldsymbol{L}_{\boldsymbol{P}})$ as a quadratic function of $\mathfrak{M}$ via a Legendre transformation on $\boldsymbol{L}_{\boldsymbol{P}}$ and enforcing the Principle of Maximum Dissipation (Hackl and Fischer, 2008). Setting $\mathfrak{D}=\check{\mathfrak{D}}(\boldsymbol{C},\boldsymbol{P},\mathfrak{M})=-\mathfrak{M}:\check{\mathbb{K}}(\boldsymbol{F},\boldsymbol{P}):\mathfrak{M}$, we have

$$\boldsymbol{L}_{\boldsymbol{P}}=-\frac{1}{2}\frac{\partial\check{\mathfrak{D}}}{\partial\mathfrak{M}}=-\check{\mathbb{K}}(\boldsymbol{F},\boldsymbol{P}):\mathfrak{M}, \qquad (19)$$

where $\check{\mathbb{K}}(\boldsymbol{F},\boldsymbol{P})$ is a fourth-order tensor with major symmetry only. For the purpose of this work, we define $\check{\mathbb{K}}(\boldsymbol{F},\boldsymbol{P})$ as $\check{\mathbb{K}}(\boldsymbol{F},\boldsymbol{P})=k\,\boldsymbol{b}_{\boldsymbol{P}}\underline{\otimes}\,\boldsymbol{c}_{\boldsymbol{P}}$ (with components $k\,(\boldsymbol{b}_{\boldsymbol{P}})^{AC}\,(\boldsymbol{c}_{\boldsymbol{P}})_{BD}$), the "tensor-down" product $\underline{\otimes}$ is defined in Curnier et al., 1995), with k being a positive constant, and $\boldsymbol{b}_{\boldsymbol{P}}=\boldsymbol{P}\,\mathfrak{g}^{-1}\boldsymbol{P}^T$ and $\boldsymbol{c}_{\boldsymbol{P}}=\boldsymbol{b}_{\boldsymbol{P}}^{-1}$ being the "left Cauchy-Green tensor" and the "Finger tensor" associated with $\boldsymbol{P}$, respectively. Moreover, in order to enforce a deviatoric $\boldsymbol{L}_{\boldsymbol{P}}$ (no growth), we make it function of the deviatoric Mandel stress $\mathfrak{M}_d=\mathfrak{M}-\frac{1}{3}(\boldsymbol{I}:\mathfrak{M})\boldsymbol{I}^T$, i.e.,

$$\boldsymbol{L}_{\boldsymbol{P}}=-k\,\boldsymbol{b}_{\boldsymbol{P}}\mathfrak{M}_d\boldsymbol{c}_{\boldsymbol{P}}, \qquad (20)$$

which can be shown to respect condition (17).

6. Example: Application to the Arterial Wall

Here, we apply our recruitment-reorientation remodelling framework to the benchmark problem reported by Olsson and Klarbring (2008) and Grillo et al. (2015), with a cylinder reinforced by two families of fibres (mimicking the arterial wall) under plane strain in the plane orthogonal do the direction $X^3\equiv Z$ of the axis of the cylinder.

Fibre Implant. At each material point, we implant an archetypal distribution with dominant direction $\boldsymbol{\mu}_0=0\,\mathfrak{a}_1+0\,\mathfrak{a}_2+1\,\mathfrak{a}_3$ into two families of fibres with equal and opposite angles, γ and $-\gamma$, measured from the Z-direction in the Θ-Z-plane and corresponding to the material directions $\boldsymbol{M}_{0+}$ and $\boldsymbol{M}_{0-}$, as shown in Figure 2. This amounts to defining an implant tensor $\boldsymbol{P}$ and then adapting its expression to the two angles γ and $-\gamma$, which gives the implants $\boldsymbol{P}_+$ and $\boldsymbol{P}_-$, respectively. The polar decomposition

$\boldsymbol{P} = \boldsymbol{R}\boldsymbol{U}$ of the implant (Equation (3)) yields

$$[\![\boldsymbol{U}]\!] = \begin{bmatrix} \sqrt{\lambda_s} & 0 & 0 \\ 0 & \sqrt{\lambda_s} & 0 \\ 0 & 0 & \lambda_s^{-1} \end{bmatrix}, \quad [\![\boldsymbol{R}]\!] = \begin{bmatrix} 1 & 0 & 0 \\ 0 & \cos\gamma & \sin\gamma \\ 0 & -\sin\gamma & \cos\gamma \end{bmatrix}. \tag{21}$$

Fibre Orientation Probability. In each family, the fibre orientation follows a *bivariate* von Mises distribution (Holzapfel et al., 2015; Gizzi et al., 2018), in which we set the constants so to normalise it to one, i.e.,

$$\check{\Psi}(\beta, \alpha) = \sqrt{\frac{2b}{\pi}} \frac{\exp(a\cos 2\alpha)\exp(b(1+\cos 2\beta))}{2\pi I_0(a)\ \mathrm{erfi}(\sqrt{2b})}, \tag{22}$$

where α and β are the archetypical longitude and co-latitude angle, erfi is the *imaginary error function* and I_0 is the *Bessel function* of zero kind (see Abramowitz and Stegun, 1964). In this study, we used the values $a = -1$ and $b = 5$ of the concentration parameters, to obtain fibres mostly laying in the Θ-Z-plane, as illustrated in Figure 2.

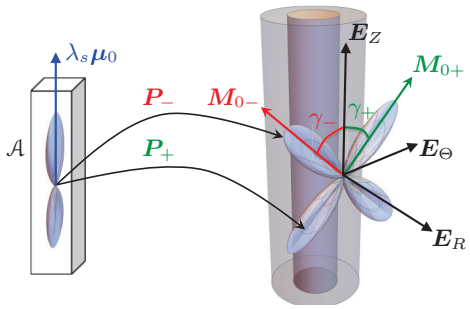

Figure 2: Tensors $\boldsymbol{P}_+$ and $\boldsymbol{P}_-$, with identical expressions except for the angles γ and $-\gamma$, respectively, implant the two fibre families, described by $\boldsymbol{M}_{0+}$ and $\boldsymbol{M}_{0-}$, from the archetypal straight state, described by $\lambda_s\boldsymbol{\mu}_0$.

Deformation. We cover the body manifold with a polar chart, denoted by (R, Θ, Z), in which, $R \in [R_i, R_o]$, $\Theta \in [0, 2\pi]$, $Z \in [0, L]$. Here, R_i and R_o, are the inner and outer radii respectively, Θ is the referential polar angle and L is the length of the cylinder. The current configuration is obtained under the assumption of pure inflation as:

$$(R, \Theta, Z) \mapsto (r, \theta, z) = (\chi^r(R, t), \Theta, Z). \tag{23}$$

For convenience, from this point forward, we write $\xi \equiv \chi^r$. Since ξ is a function solely of the radial coordinate R and time, we denote $\xi' \equiv \partial\chi^r/\partial R$. The orthonormal bases for the tangent spaces of the referential and the current configurations are denoted by $\{\boldsymbol{E}_R, \boldsymbol{E}_\Theta, \boldsymbol{E}_Z\}$ and $\{\boldsymbol{e}_r, \boldsymbol{e}_\theta, \boldsymbol{e}_z\}$, respectively. Thus, the deformation gradient $\boldsymbol{F}$ reads

$$\boldsymbol{F}(R, t) = \xi'(R, t)\, \boldsymbol{e}_r \otimes \boldsymbol{E}^R + \frac{\xi(R, t)}{R}\, \boldsymbol{e}_\theta \otimes \boldsymbol{E}^\Theta + \boldsymbol{e}_z \otimes \boldsymbol{E}^Z. \tag{24}$$

Imposing incompressibility, i.e., $J = \det \boldsymbol{F} = 1$, we have

$$\xi'(R, t)\xi(R, t) = R. \tag{25}$$

Note that the condition $J = 1$, together with the restriction $J_{\boldsymbol{P}} = 1$, amounts to require that also the tensor $\boldsymbol{F}\boldsymbol{P}$ has unitary determinant.

The separable differential equation (25) has solution

$$\xi(R, t) = \sqrt{R^2 + \upsilon(t)}, \tag{26}$$

in which the function υ is *independent* of R and has to be determined from the boundary conditions. Note that, in order for $\xi(R, t)$ to be well defined, $\upsilon(t)$ must be bounded from below, i.e., it must hold $\upsilon(t) \geq -R_i^2$, for all t. Also, we have

$$\xi'(R, t) = \frac{R}{\sqrt{R^2 + \upsilon(t)}} = \frac{R}{\xi(R, t)}, \tag{27}$$

so that the matrix representation of $\boldsymbol{F}$ is

$$[\![\boldsymbol{F}(R, t)]\!] = \begin{bmatrix} \frac{R}{\xi(R,t)} & 0 & 0 \\ 0 & \frac{\xi(R,t)}{R} & 0 \\ 0 & 0 & 1 \end{bmatrix}. \tag{28}$$

Constitutive Equations. Following the premises in Section 4, the artery is modelled as hyperelastic with an isotropic matrix contribution $\hat{W}_m$, an isotropic fibre contribution $\hat{W}_{fi}$ and an anisotropic fibre contribution $\hat{W}_{e\pm}$, integral of the anisotropic fibre contribution $\hat{W}_{fa\pm}$, based on the ensemble potential $\hat{W}_e$ introduced in (13). Thus,

$$\begin{aligned} \hat{W}(\boldsymbol{C}, X) = (1 - \Phi_f)\hat{W}_m(\boldsymbol{C}) + \\ + \Phi_f(\hat{W}_{fi}(\boldsymbol{C}) + \hat{W}_{e+}(\boldsymbol{C}, X) + \hat{W}_{e-}(\boldsymbol{C}, X)), \end{aligned} \tag{29}$$

where Φ_f is the fibre volumetric fraction, assumed homogeneous through the sample, and

$$\hat{W}_m(\boldsymbol{C}) = \tfrac{1}{2}k_m[\hat{I}_1 - 3], \tag{30a}$$

$$\hat{W}_{fi}(\boldsymbol{C}) = \tfrac{1}{2}k_{fi}[\hat{I}_1 - 3], \tag{30b}$$

$$\hat{W}_{fa\pm}(\boldsymbol{C}, X) = \tfrac{1}{4}k_{fa}\ \mathcal{H}(\hat{I}_{4\pm}(X) - 1)[\hat{I}_{4\pm}(X) - 1]^2, \tag{30c}$$

where $\hat{I}_1 = \mathrm{tr}(\boldsymbol{C})$ and the step function $\mathcal{H}$ is needed to "switch-off" fibres with stretch smaller than one. The second Piola-Kirchhoff stress is obtained as $\boldsymbol{S} = 2\,\partial\hat{W}/\partial\boldsymbol{C}$ and, in particular, the anisotropic ensemble contribution is given by

$$\boldsymbol{S}_{e\pm} = J_{\boldsymbol{P}}^{-1} \int_{\mathbb{S}^2} 2\, \frac{\partial\check{W}_{fa\pm}}{\partial\check{I}_{4\pm}} \frac{\partial\check{I}_{4\pm}}{\partial\boldsymbol{C}}\, \check{\Psi}(\boldsymbol{\mu}), \tag{31}$$

where we used (14) to transform $\hat{W}_{fa\pm}$ into $\check{W}_{fa\pm}$ and

$$\frac{\partial\check{I}_{4\pm}}{\partial\boldsymbol{C}} = \frac{\partial(\boldsymbol{P}_\pm^T\boldsymbol{C}\boldsymbol{P}_\pm : \boldsymbol{\mu}\otimes\boldsymbol{\mu})}{\partial\boldsymbol{C}} = \boldsymbol{P}_\pm^T \underline{\otimes} \boldsymbol{P}_\pm^T : \boldsymbol{\mu}\otimes\boldsymbol{\mu}, \tag{32}$$

with components $(\boldsymbol{P}_\pm)^A{}_\alpha(\boldsymbol{P}_\pm)^B{}_\beta\,\mu^\alpha\mu^\beta$ (see Curnier et al., 1995, for the definition of the "tensor-down" product $\underline{\otimes}$).

In order to enforce the incompressibility constraint, we employ the pulled-back deviatoric part (see Federico, 2012) of the second Piola-Kirchhoff stress,

$$\boldsymbol{S}_d \equiv \mathrm{Dev}^*\boldsymbol{S} = \boldsymbol{S} - \tfrac{1}{3}(\boldsymbol{C} : \boldsymbol{S})\,\boldsymbol{C}^{-1}. \tag{33}$$

We emphasise that, since we consider that the elastic potential of the matrix does not evolve and we have two families of fibres with different implants, we only consider the fibre part of the deviatoric Mandel stress as the driving force of evolution, i.e.,

$$\mathfrak{M}_{ed\pm} = \mathrm{Dev}\,(\boldsymbol{C}\boldsymbol{S}_{e\pm}) = \boldsymbol{C}\boldsymbol{S}_{e\pm} - \tfrac{1}{3}(\boldsymbol{I} : \boldsymbol{C}\boldsymbol{S}_{e\pm})\boldsymbol{I}^T. \quad (34)$$

Equilibrium, Boundary Conditions, Integration. The cylinder is under uniform pressure $\wp$ on the inner boundary $\partial\mathcal{B}_i$ and and zero traction on the outer boundary $\partial\mathcal{B}_o$, and body force and inertial effects are neglected. Thus, the evolution of the tissue is governed by the equation for $\boldsymbol{P}$, given in (17) and equipped with appropriate initial conditions, and by the boundary value problem

$$\begin{aligned} \mathrm{Div}\,\boldsymbol{T} &= \boldsymbol{0}, && \text{in } \mathcal{B}. && (35a)\\ \boldsymbol{T}\,\boldsymbol{N} &= -J\,\wp\,\boldsymbol{F}^{-T}, && \text{on } \partial\mathcal{B}_i, && (35b)\\ \boldsymbol{T}\,\boldsymbol{N} &= \boldsymbol{0}, && \text{on } \partial\mathcal{B}_o, && (35c) \end{aligned}$$

where $\boldsymbol{N}$ is the normal covector to the boundary $\partial\mathcal{B}$, and the hypothesis of isochoric deformation implies $J = 1$.

Since we consider an axisymmetric problem, the first Piola-Kirchhoff stress is independent of Θ and Z. Also, the boundary conditions ensure that the matrix associated with the first Piola-Kirchhoff stress is diagonal, i.e., $[\![\boldsymbol{T}]\!] = \mathrm{diag}[{T_r}^R, {T_\theta}^\Theta, {T_z}^Z]$. The first Piola-Kirchhoff stress can be expressed as the sum of its hydrostatic and deviatoric components, and in terms of the deviatoric second Piola-Kirchhoff stress, as

$$\boldsymbol{T} = \boldsymbol{T}_h + \boldsymbol{T}_d = -J\,p\,\boldsymbol{F}^{-T} + \boldsymbol{g}\,\boldsymbol{F}\,\boldsymbol{S}_d. \quad (36)$$

The hydrostatic pressure p is found from (35) (see Grillo et al., 2015).

Evolution Equation. The evolution equation for each of the $\dot{\boldsymbol{P}}_\pm$ is obtained from that of $\boldsymbol{L}_{\boldsymbol{P}_\pm} = \dot{\boldsymbol{P}}_\pm \boldsymbol{P}_\pm^{-1}$ by right-multiplying Equation (20) written for each $\boldsymbol{P}_\pm$, by the corresponding $\boldsymbol{P}_\pm$

$$\dot{\boldsymbol{P}}_\pm = -k\; J_{\boldsymbol{P}_\pm}\, \boldsymbol{P}_\pm\, \mathfrak{g}^{-1} \boldsymbol{P}_\pm^T \mathfrak{M}_{ed\pm} \boldsymbol{P}_\pm^{-T} \mathfrak{g}. \quad (37)$$

In our example, using (3) and (21), solving Equation (37) for the deviatoric Mandel stress $\mathfrak{M}_{ed\pm}$ of each of the two fibre families, and then summing to obtain the overall deviatoric Mandel stress of the fibres $\mathfrak{M}_{ed}$, yields

$$\begin{aligned} \tfrac{\dot{\lambda}_s}{\lambda_s} &= k\,(\mathfrak{M}_{ed})_R{}^R, && (38a)\\ \tfrac{\frac{1}{2}\lambda_s^2(3\cos(2\gamma)-1)\dot{\lambda}_s - \left(\lambda_s^6-1\right)\dot{\gamma}\sin(2\gamma)}{\lambda_s^3} &= k\,(\mathfrak{M}_{ed})_\Theta{}^\Theta. && (38b) \end{aligned}$$

Numerical Algorithm. To study the numerical example discussed in the previous sections, a code is developed in *Wolfram Mathematica*. The main focus of the numerical algorithm in this study is to have high *accuracy* and *precision* as we are studying a model with a simple geometry (isochoric inflation of a hollow cylinder). Although the geometry is simple, the evolution equation (38) makes the model computationally heavy. In this numerical study, we have two types of integrals: the surface integral over the unit sphere $\mathbb{S}^2$, which describes the fibre distribution, and the integral over the interval bounded by the inner and the outer radii $[R_i, R_o]$. For the surface integral, we use the *Lebedev quadrature* (Lebedev, 1977), in which the grid points and the corresponding weights are obtained from the exact integration of *spherical harmonics* up to an arbitrary order. The model parameters are given in Table 1.

Parameter	Value	Symbol
inner radius	1 mm	R_i
outer radius	2 mm	R_o
internal pressure	0.02 MPa	$\wp_i$
initial angle	$\pi/4$	γ_0
initial λ_s	1.014	λ_{s0}
matrix stiffness	0.0375 MPa	k_m
fibre isotropic stiffness	0.0375 MPa	k_{fi}
fibre anisotropic stiffness	0.0375 MPa	k_{fa}
remodelling stiffness	5×10^{-8} s/Pa	k
fibre volume fraction	0.2	Φ_f

Table 1: Parameters employed in the numerical analysis.

7. Numerical Results

Figure 3 represents the evolution of the straightening stretch λ_s. The behaviour of λ_s is monotonically decreasing in the radius R throughout the evolution. The difference $\lambda_s(R_i, t) - \lambda_s(R_o, t)$ increases monotonically with time. We note that the $\lambda_s(R_o)$ evolves due to the fact that the radial deviatoric Mandel stress of the fibres, $\mathfrak{M}_{ed}$ is not zero (Equation (38)), although the total Mandel stress $\mathfrak{M}$ vanishes due to the boundary conditions.

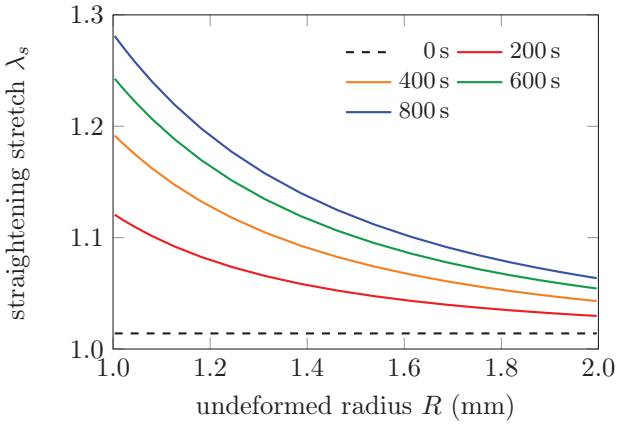

Figure 3: Evolution of the straightening stretch λ_s with time.

Figure 4 shows the evolution of the behaviour of the angle γ describing the preferred fibres direction with time. After remodelling, the maximum and minimum angles occur at the inner and outer radii, respectively. The differ-

ence $\gamma(R_i,t) - \gamma(R_o,t)$ is more pronounced in the early cycles and then tends to remain constant with time.

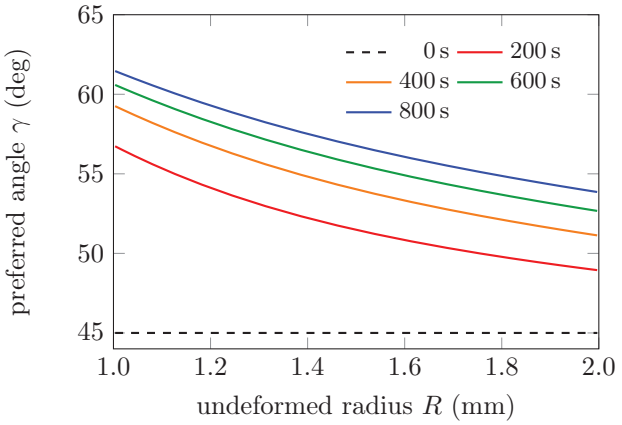

Figure 4: Evolution of the preferred fibre angle γ with time.

Figure 5 shows the evolution of the radial first Piola-Kirchhoff stress ${T_r}^R$ (dashed lines) and circumferential first Piola-Kirchhoff stress ${T_\theta}^\Theta$ (solid lines) as a function of the deformed radius $r = \xi(R,t)$. The remodelling makes the circumferential stress ${T_\theta}^\Theta$ more homogeneous throughout the thickness of the tube. The difference ${T_\theta}^\Theta(R_i,t) - {T_\theta}^\Theta(R_o,t)$ before remodelling is about 23 kPa at $t = 0\,\mathrm{s}$ and it reduces to 16 kPa at $t = 400\,\mathrm{s}$ and to 14 kPa at $t = 800\,\mathrm{s}$.

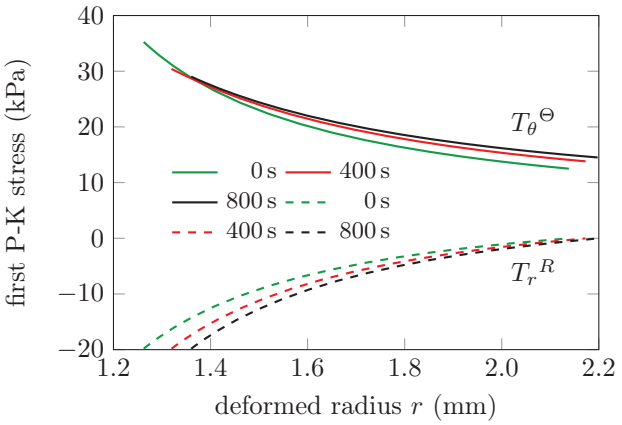

Figure 5: First Piola-Kirchhoff stresses ${T_r}^R$ (dashed lines) and ${T_\theta}^\Theta$ (solid lines).

One of the most prominent mechanical aspects of biological tissues is the presence of residual stresses. Fung (1983) predicted that the distribution of residual stresses in the arteries is such that the residual circumferential stress (along Θ-axis) is compressive in the interior layers and tensile in the outer ones. The residual second Piola-Kirchhoff stresses for our benchmark problem is shown in Figure 6 as a function of the undeformed radius R, at time $t = 800\,\mathrm{s}$. All three principal residual stresses increase monotonically and the residual circumferential stress $S^{\Theta\Theta}$, in accordance with Fung (1983), is compressive at the inner wall and tensile at the outer wall.

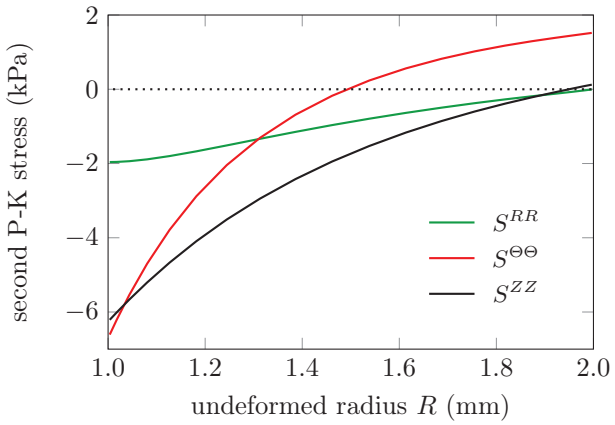

Figure 6: Residual second Piola-Kirchhoff stresses at time $t = 800\,\mathrm{s}$.

8. Discussion and Conclusions

In this work we introduced a thermodynamically admissible model for pure remodelling of a fibre-reinforced material representing the arterial wall tissue. The approach is based on the theory of material uniformity, which is described by the material implant $\boldsymbol{P}$. We proposed a simple evolution law, in which the inhomogeneity rate $\boldsymbol{L_P}$ is linearly related to the *deviatoric Mandel stress* $\mathfrak{M}_d$.

Using the evolution law (38), we solved a benchmark numerical problem describing a pressurised thick-walled cylinder under plane strain conditions, with uniform internal pressure, as in the works by Olsson and Klarbring (2008) and Grillo et al. (2015). We use the same constitutive laws as in the work by Grillo et al. (2015) but a more realistic fibre orientation probability, with two families of fibres each obeying a bivariate von Mises distribution (Holzapfel et al., 2015; Gizzi et al., 2018) (Figure 2).

The results for the remodelling angle are qualitatively similar to those obtained by Grillo et al. (2015). Both models predict that the preferred angle γ increases with time, with values at the inner radius R_i being the largest. Moreover, the dependence on radius and time of the *radial* and *circumferential* stresses ${T_r}^R$ and ${T_\theta}^\Theta$ in our model (Figure 5) is similar to that in the paper by Grillo et al. (2015). However, while in Grillo et al. (2015) the cylinder deflates as it becomes stiffer *circumferentially*, in our study the cylinder inflates. This is not surprising, as we have *two* evolving mechanisms that work simultaneously, namely the relaxation of the fibres (increasing straightening stretch λ_s) and the change in fibre angle (increasing preferred angle γ). Indeed, when λ_s increases, it causes a *relaxation* of the fibres, and the cylinder needs to inflate so that the fibres reach their straightening stretch and are able to bear load.

Other studies considered a change of undulation of the fibres or fibrils and our model is in agreement with these

findings, despite being fundamentally different in the basic assumptions. Indeed, Humphrey (1999) considers resorption and deposition of new fibres and Watton and Hill (2009) and Watton et al. (2009) consider pre-stretch in Z-direction. The relaxation effect that our model predicts has been observed by Kamiya and Togawa (1980). In addition, the residual stress is compressive in the inner layer and tensile in the outer layer, in agreement with the behaviour described by Fung (1983).

It is noteworthy that, in our model, we did not prescribe the evolution law in accordance to experimental observations. Rather, we postulated an evolution law solely based on the conditions of reduction to the archetype (17) and of compliance with the dissipation inequality (18). In spite of its relatively simple form, the evolution law could qualitatively reproduce the remodelling behaviour seen in other studies. This indicates that the framework based on the theory of evolution and material uniformity can be a viable and promising paradigm to explore growth and remodelling of biological tissues.

This work followed Epstein and Maugin (2000) and Epstein and Elzanowski (2007), who used the theory of uniformity with a time-dependent implant $\boldsymbol{P}$, which constitutes an *internal variable*. In contrast, Grillo et al. (2015) treated the fibre mean angle as a kinematic variable that satisfies a balance of generalised forces, following the same philosophy used by Di Carlo and Quiligotti (2002). Although different in nature, these two approaches give qualitatively similar results.

The proposed model constitutes a step further in the study of growth and remodelling of fibre-reinforced soft biological tissues, in the framework of material implant theory. Even though the numerical example lacks the necessary details to study specific cases such as *hypertension* and *aneurysms*, the agreements of the results with previous studies make this framework promising.

Acknowledgements

This work was supported in part by the Natural Sciences and Engineering Research Council of Canada, through the NSERC Discovery Programme [SF,ME], and the Dipartimento di Eccellenza 2018-2022, Politecnico di Torino (Italy), Project no. E11G18000350001 [AG].

Competing Interests

The authors declare no competing interests.

References

Abramowitz, M., Stegun, I.A., 1964. Handbook of mathematical functions: with formulas, graphs, and mathematical tables. volume 55. Courier Corporation.

Cleja-Tigoiu, A., Maugin, G.A., 2000. Eshelby's stress tensors in finite elastoplasticity. Acta Mechanica 139, 231–249.

Cowin, S., Hegedus, D., 1976. Bone remodeling I: theory of adaptive elasticity. Journal of Elasticity 6, 313–326.

Crevacore, E., Di Stefano, S., Grillo, A., 2018. Coupling among deformation, fluid flow, structural reorganisation and fibre reorientation in fibre-reinforced, transversely isotropic biological tissues. Int. J. Non-Linear Mech. DOI:10.1016/j.ijnonlinmec.2018.08.022., 1–14.

Curnier, A., He, Q.C., Zysset, P., 1995. Conewise linear elastic materials. J. Elasticity 37, 1–38.

Di Carlo, A., Quiligotti, S., 2002. Growth and balance. Mech. Res. Commun. 29, 449–456.

Di Stefano, S., Ramirez-Torres, A., Penta, R., Grillo, A., 2018. Self-influenced growth through evolving material inhomogeneities. Int. J. Non-Linear Mech. 106, 174–187.

Epstein, M., Elzanowski, M., 2007. Material inhomogeneities and their evolution: a geometric approach. Springer Science & Business Media.

Epstein, M., Maugin, G.A., 1990. The energy-momentum tensor and material uniformity in finite elasticity. Acta Mech. 83, 127–133.

Epstein, M., Maugin, G.A., 2000. Thermomechanics of volumetric growth in uniform bodies. Int. J. Plasticity 16, 951–978.

Federico, S., 2012. Covariant formulation of the tensor algebra of non-linear elasticity. Int. J. Non Lin. Mech. 47, 273–284.

Federico, S., Herzog, W., 2008. Towards an analytical model of soft tissues. J. Biomech. 41, 3309–3313.

Fung, Y.C., 1983. On the foundations of biomechanics. J. Appl. Mech. 50, 1003–1009.

Gizzi, A., Pandolfi, A., Vasta, M., 2018. A generalized statistical approach for modeling fiber-reinforced materials. Journal of Engineering Mathematics 109, 211–226.

Grillo, A., Carfagna, M., Federico, S., 2018. An Allen-Cahn approach to the remodelling of fibre-reinforced anisotropic materials. Journal of Engineering Mathematics 109, 139–172.

Grillo, A., Wittum, G., Tomic, A., Federico, S., 2015. Remodelling in statistically oriented fibre-reinforced materials and biological tissues. Math. Mech. Solids 20, 1107–1129.

Gurtin, M.E., 1999. Configurational forces as basic concepts of continuum physics. volume 137. Springer Science & Business Media.

Hackl, K., Fischer, F.D., 2008. On the relation between the principle of maximum dissipation and inelastic evolution given by dissipation potentials. Proc. Roy. Soc. Lond. A , 117–132.

Hamedzadeh, A., Gasser, T.C., Federico, S., 2018. On the constitutive modelling of recruitment and damage of collagen fibres in soft biological tissues. Eur. J. Mech. A/Solids 72, 483–496.

Hegedus, D.M., Cowin, S.C., 1976. Bone remodeling, II: Small strain adaptive elasticity. J. Elasticity 6, 337–352.

Hoger, A., 1997. Virtual configurations and constitutive equations for residually stressed bodies with material symmetry. J. Elasticity 48, 125–144.

Holzapfel, G.A., Niestrawska, J.A., Ogden, R.W., Reinisch, A.J., Schriefl, A.J., 2015. Modelling non-symmetric collagen fibre dispersion in arterial walls. J. R. Soc. Interface 12, 20150188.

Humphrey, J.D., 1999. Remodeling of a collagenous tissue at fixed lengths. J. Biomech. Eng. 121, 591–597.

Imatani, S., Maugin, G.A., 2002. A constitutive model for material growth and its application to three-dimensional finite element analysis. Mech. Res. Commun. 29, 477–483.

Kamiya, A., Togawa, T., 1980. Adaptive regulation of wall shear stress to flow change in the canine carotid artery. Am. J. Physiol. 239, H14–H21.

Koks, D., 2006. Explorations in mathematical physics: the concepts behind an elegant language. Springer Science & Business Media.

Lebedev, V., 1977. Spherical quadrature formulas exact to orders 25–29. Siberian Mathematical Journal 18, 99–107.

Noll, W., 1967. Materially uniform simple bodies with inhomogeneities. Arch. Rat. Mech. Anal. 27, 1–32.

Olsson, T., Klarbring, A., 2008. Residual stresses in soft tissue as a consequence of growth and remodeling: application to an arterial geometry. European Journal of Mechanics-A/Solids 27, 959–974.

Rodriguez, E.K., Hoger, A., McCulloch, A.D., 1994. Stress-dependent finite growth in soft elastic tissues. J. Biomech. 27, 455–467.

Simo, J.C., 1988. A framework for finite strain elastoplasticity based

on maximum plastic dissipation and the multiplicative decomposition: Part I. Continuum formulation. Comput. Meth. Appl. Mech. Eng. 66, 199–219.

Simo, J.C., Hughes, T.J.R., 1986. On the variational foundations of assumed strain methods. J. Appl. Mech. 53, 51–54.

Watton, P., Hill, N., 2009. Evolving mechanical properties of a model of abdominal aortic aneurysm. Biomechanics and modeling in mechanobiology 8, 25–42.

Watton, P.N., Hill, N.A., Heil, M., 2004. A mathematical model for the growth of the abdominal aortic aneurysm. Biomech. Model. Mechanobiol. 3, 98–113.

Watton, P.N., Ventikos, Y., Holzapfel, G.A., 2009. Modelling the growth and stabilization of cerebral aneurysms. Mathematical medicine and biology 26, 133–164.